

Optimization of Resonant Λ -type Quantum Memory with Gaussian Pulses

Kai Shinbrough^{1,*}, Benjamin Hunt¹, and Virginia O. Lorenz¹
¹*Department of Physics, University of Illinois at Urbana-Champaign,
 1110 West Green Street, Urbana, IL 61801, USA*
 (August 31, 2020)

Optical quantum memory—the ability to store photonic quantum states and retrieve them on demand—is an essential resource for emerging quantum technologies and photonic quantum information protocols. Simultaneously achieving high efficiency and high-speed, broadband operation is an important task necessary for enabling these applications. In this work, we investigate the optimization of a large class of optical quantum memory protocols based on resonant interaction with ensembles of Λ -type level systems with the restriction that the temporal envelope of all optical fields must be Gaussian, which reduces experimental complexity. We show that for overlapping signal and control fields there exists a unique and broadband pulse duration that optimizes the memory efficiency, and that this optimized efficiency can be close to the protocol-independent bound. We further optimize over the control field temporal delay and pulse duration, demonstrating saturation of this efficiency bound over a broad range of pulse durations while clarifying the underlying physics of the quantum memory interaction.

I. INTRODUCTION

Efficient photonic quantum state generation and synchronization [1, 2], metropolitan-scale quantum networking and entanglement distribution [3, 4], and linear-optical quantum computing [5] all rely on efficient optical quantum memory. In order for these emerging applications to operate at high speed they must be compatible with broadband photonic quantum states [6, 7], ideally with minimal experimental complexity and technological overhead. In quantum memories based on atomic ensembles, a significant body of theoretical [8–11] and experimental [12–14] work has been dedicated to improving quantum memory efficiency by shaping the signal field to be stored or the control field used to mediate the interaction; however, these techniques have largely only been applied for signal bandwidths smaller than the linewidths of the excited states participating in the memory interaction. In effect, ensemble quantum memories to date have been limited to efficient narrowband operation [15–19] or inefficient broadband operation [6, 20–26].

In this work, we provide a quantitative performance analysis of resonant Λ -type quantum memories, shown in Figure 1, with a specific focus on signal bandwidths of the same order or larger than the memory’s intermediate excited state linewidth ($|2\rangle$ in Fig. 1). While a variety of other level systems are employed for quantum memory (ladder-type, M -type, etc.), Λ -type level systems are currently the most common, and our analysis is readily generalizable to other level systems. In the broadband regime, where the signal field bandwidth is larger than the intermediate state linewidth, off-resonant quantum memory protocols are well-established, but require significantly more control field power than resonant protocols and suffer from low efficiency due to the difficulty of satisfying this requirement [20–23, 26]. In this

work, we restrict ourselves only to the use of resonant, Gaussian optical fields to avoid the experimental complexity of large pulse energies and shaping of the optical fields. Despite the shape restriction, we find that optimization of Gaussian control fields leads to surprisingly significant enhancement of memory efficiency, particularly in the broadband regime. We provide physical intuition for the results of our optimization in terms of the physical phenomena and quantum storage mechanisms of electromagnetically-induced transparency (EIT) [27–29] and the recently-proposed Autler-Townes splitting (ATS) quantum memory protocol [30–32]. In this way, our work paves the way for experimentally simple control field optimization in the largely unexplored broadband regime.

While in principle both the signal and control fields can be modified in order to optimize the memory performance, we consider the more typically relevant approach of optimization via the control field. Optimization of a Gaussian control field is necessarily limited in scope—there exist only three parameters subject to optimization: pulse area, or equivalently the peak Rabi frequency of the optical field; temporal delay relative to the signal field; and pulse bandwidth. There exists also the possibility to temporally chirp the optical field and optimize over control pulse duration, but in this work we consider only Fourier-transform-limited pulses.

After providing some details on our numerical analysis of the equations of motion describing the quantum memory interaction in Section II, in Section III we consider two cases of Gaussian control field optimization: (1) the naïve case of overlapping signal and control fields of the same duration, where the only optimization occurs over the control field pulse area, and (2) the full optimization of Gaussian control fields over all parameters (pulse area, temporal delay, and bandwidth).

In what follows, we assume ‘backward retrieval’ of the signal field (see Fig. 1) and that the atomic dynamics during retrieval are the time reverse of those during the stor-

* kais@illinois.edu

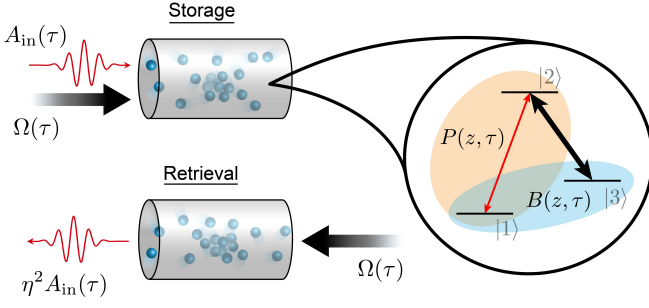


FIG. 1. ‘Backward retrieval’ quantum memory scheme, wherein a weak signal field $[A_{\text{in}}(\tau)]$, red thin line and strong control field $[\Omega(\tau)]$, black thick line enter an atomic medium, generating atomic polarization $[P(z, \tau)]$, orange ellipse and spin wave $[B(z, \tau)]$, blue ellipse fields according to the Λ -type level scheme shown on the right. After a controllable delay, the signal field is retrieved with total efficiency η^2 via the application of another strong control field that propagates antiparallel to the first control field.

age process, which holds for near-degenerate metastable states ($|1\rangle$ and $|3\rangle$ in Fig. 1) [9, 10, 29]. In this case, the retrieval efficiency is identical to the storage efficiency, η , and the total memory efficiency is η^2 , meaning in order to fully characterize the memory efficiency we need only compute η . Since the Gaussian fields we consider are intrinsically time-reversal symmetric, under these assumptions, beyond routing the retrieval control pulse to the output facet of the atomic ensemble, no additional experimental measures need to be taken in order to ensure optimization of retrieval.

II. NUMERICAL SOLUTION OF MAXWELL-BLOCH EQUATIONS

The Λ -type level structure shown in Fig. 1 includes two stable or meta-stable ground states, $|1\rangle$ and $|3\rangle$, and an intermediate excited state $|2\rangle$ that decays to the ground states with the coherence decay rate $\gamma = \Gamma/2$, where Γ is the total radiative decay rate of level $|2\rangle$. All temporal dynamics are considered in the co-moving frame defined by $\tau = t - z/c$, where t is the time measured in the lab frame, z is the one-dimensional spatial coordinate—defined as $z = 0(L)$ at the input (output) face of the medium, where L is the length of the medium—and c is the speed of light. We assume that a strong control field with frequency centered on the $|2\rangle \leftrightarrow |3\rangle$ transition and Rabi frequency $\Omega(\tau)$ enters the medium with a Gaussian temporal envelope and does not undergo significant absorption or distortion as it propagates through the medium $[\Omega(z, \tau) = \Omega(\tau)]$. We assume that before the signal field enters the medium, it has a Gaussian temporal envelope $A_{\text{in}}(\tau) = e^{-\tau^2/4\sigma^2}$, where $\sigma = \tau_{\text{FWHM}}/(2\sqrt{2\ln 2})$, and the signal duration τ_{FWHM} [temporal full width at half maximum (FWHM)] is related to its spectral bandwidth by $\delta = 2\pi \times 2\ln 2/(\pi\tau_{\text{FWHM}})$.

The same relationship is assumed for the control field duration, $\tau_{\text{FWHM}}^{\text{ctrl}}$, and bandwidth, δ^{ctrl} . We further assume that all atoms initially populate the $|1\rangle$ state, which is a valid approximation for atomic populations after optical pumping, or for atomic species with large energy separation between the $|1\rangle$ state and other low-lying states. In general, the signal field undergoes spatial and temporal deformation as it propagates through the medium and is absorbed along the $|1\rangle \rightarrow |2\rangle$ transition, described by $A(z, \tau)$. The atomic dynamics in the presence of these two optical fields are described by the resonant, normalized Maxwell-Bloch equations [9, 30, 33]:

$$\partial_z A(z, \tau) = -\sqrt{d}P(z, \tau) \quad (1)$$

$$\partial_\tau P(z, \tau) = -\gamma P(z, \tau) + \sqrt{d}A(z, \tau) - i\frac{\Omega(\tau)}{2}B(z, \tau) \quad (2)$$

$$\partial_\tau B(z, \tau) = -\gamma_B B(z, \tau) - i\frac{\Omega^*(\tau)}{2}P(z, \tau), \quad (3)$$

where d is the resonant optical depth of the memory and $P(z, \tau)$ and $B(z, \tau)$ are macroscopic field operators representing the atomic coherences $|1\rangle \leftrightarrow |2\rangle$ and $|1\rangle \leftrightarrow |3\rangle$, respectively, which are delocalized across the length of the medium. We assume that the coherence decay rate corresponding to the $|3\rangle \leftrightarrow |1\rangle$ transition, γ_B , is negligible in comparison to the excited state decay rate: $\gamma_B \ll \gamma$.

We iteratively solve these equations of motion using Heun’s method for evaluating the τ -derivatives and Chebyshev differentiation for the z -derivatives. After integration, we compare the population in B to the population in A_{in} in order to calculate the storage efficiency for a particular choice of $\Omega(\tau)$, as:

$$\eta = \frac{\int_0^L dz |B(z, \tau \rightarrow \infty)|^2}{\int_{-\infty}^{\infty} d\tau |A_{\text{in}}(\tau)|^2}, \quad (4)$$

where in practice we truncate $A_{\text{in}}(\tau)$ and $B(z, \tau)$ at $\tau^{\text{end}} = 4\tau_{\text{FWHM}}$, where $A_{\text{in}}(\tau^{\text{end}})$ has dropped to $\mathcal{O}(10^{-10})$ of its maximum value. Thus equations (1)-(3) in combination with equation (4) define an objective function that can be maximized with respect to the free parameters of $\Omega(\tau)$. We parameterize the control field Rabi frequency—which we take to be real for simplicity—in terms of its pulse area $\theta = \int_{-\infty}^{\infty} d\tau \Omega(\tau)$, temporal delay $\Delta\tau^{\text{ctrl}}$ relative to the arrival of the signal field, and duration $\tau_{\text{FWHM}}^{\text{ctrl}} = 2\sqrt{2\ln 2}\sigma^{\text{ctrl}}$ as:

$$\Omega(\tau) = \Omega_0 e^{-[(\tau - \Delta\tau^{\text{ctrl}})/2\sigma^{\text{ctrl}}]^2}, \quad (5)$$

where $\Omega_0 = \theta/(2\sqrt{\pi}\sigma^{\text{ctrl}})$, and we optimize over the above parameters using a Nedler-Mead simplex method. For simplicity we define $\tau = 0$ at the maximum of the signal field; this implies that positive values of the control field delay ($\Delta\tau^{\text{ctrl}} > 0$) refer to control fields arriving after the signal field.

III. RESULTS

We first consider the case of overlapping signal and control fields having the same bandwidth and no temporal delay. In this naïve scheme, the only experimental optimization of the memory occurs over the control field pulse area, or optical power. The results for this restricted optimization scheme are shown in the thin lines of Fig. 2(a) and the upper panel of Fig. 2(b), where we quantify the memory performance in terms of the storage efficiency, η , normalized by the protocol-independent efficiency bound imposed by finite optical depth, η_{\max} [9]. We consider η/η_{\max} as a function of the signal field duration, τ_{FWHM} , given in units of the excited state linewidth, $1/\gamma$. We consider optical depths $d = 1, 5, 10, 50$, which we take to be representative of the bulk of experimental quantum memories, but the results discussed below are equally valid for larger d , as we show in Ref. [34].

For this restricted optimization scheme we find that two physical mechanisms lead to a maximum memory efficiency at finite bandwidth. In the non-adiabatic ($d\tau_{\text{FWHM}}\gamma \lesssim 1$) and broadband ($\tau_{\text{FWHM}} \ll 1/\gamma$) regime, we find that the optimized protocol corresponds to storage via ATS [30], where the finite linewidth of the excited state limits the absorption of the signal field (i.e., population of the P field), and therefore how much population can be transferred to the storage field, B [35]. This is in contrast to the adiabatic ($d\tau_{\text{FWHM}}\gamma \gg 1$) and narrowband ($\tau_{\text{FWHM}} > 1/\gamma$) regime, where the optimized protocol corresponds to storage via EIT and the storage efficiency at finite optical depth is limited by imperfect adiabatic elimination of the P field, which leads to loss and decay back to ground state $|1\rangle$ [29, 31, 36]. In general, these competing effects—finite absorption of the signal field in the broadband regime and loss from the atomic polarization field in the narrowband regime—lead to a maximum storage efficiency at a unique value of τ_{FWHM} . The results presented in Fig. 2(b) show that in general this maximum efficiency can be close to the optimal bound ($\eta/\eta_{\max} = 100\%$), even in this naïve scheme.

We take this result to be simple and physically intuitive, but nevertheless we find it provides an important and new perspective for efficient implementation of quantum memory: For any Λ -type quantum memory parameterized by the system's excited state linewidth and optical depth—the only two physically relevant properties of the system—there exists a unique signal field pulse duration that optimizes the memory, if the Gaussian control field bandwidth and temporal delay are not optimized. The use of any other Gaussian pulse duration necessarily implies sub-optimal memory efficiency, and, particularly in the broadband regime, the choice of a signal bandwidth too large for the memory can severely limit memory efficiency.

For optical depths $d \sim 50$ and larger in this restricted optimization scheme, we observe oscillations in the optimized storage efficiency in the broadband regime [thin black curve in upper panel of Fig. 2(b)]. To under-

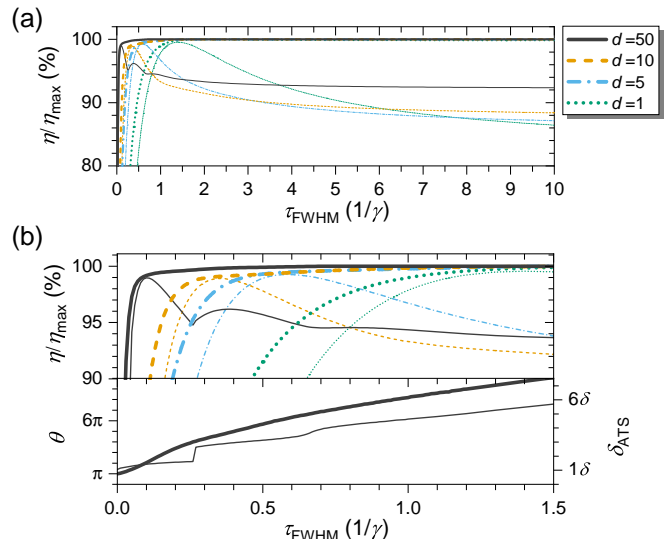


FIG. 2. (a) Normalized storage efficiency (η/η_{\max}) of Λ -type quantum memory for Gaussian control fields optimized over pulse area only (thin lines) and Gaussian control fields optimized over pulse area, temporal delay and bandwidth (thick lines) as a function of signal field duration (τ_{FWHM}) for optical depths $d = 1, 5, 10, 50$. (b) Upper: Magnification of (a) in the broadband regime. Lower: Corresponding pulse area, θ , and equivalent Autler-Townes splitting, δ_{ATS} , for $d = 50$.

stand this behavior, we analyze the optimized pulse areas, shown in the lower panel of Fig. 2(b), and the atomic dynamics presented in Fig. 3(a)-(c), which show the field intensities $|A(z, \tau)|^2$, $|P(z, \tau)|^2$, and $|B(z, \tau)|^2$ for $d = 50$, evaluated at signal field durations $\tau_{\text{FWHM}} = 0.01/\gamma$, $0.5/\gamma$, and $10/\gamma$. We identify these signal field durations, in combination with the optical depth, as representative of storage via ATS, “broadband EIT” [31], and narrowband EIT, respectively, as we now discuss.

At $\tau_{\text{FWHM}} = 0.01/\gamma$, representative of the first and largest peak amplitude of the efficiency as a function of signal duration shown in Fig. 2(b), the overlapping control field mediates the storage operation through transfer of population from the atomic polarization $P(z, \tau)$ to the spin wave field $B(z, \tau)$. Simultaneously, however, it also splits the $|1\rangle \leftrightarrow |2\rangle$ absorption feature through the Autler-Townes effect, which decreases absorption of the signal field and thus population of $P(z, \tau)$. As the Autler-Townes splitting is given by $\delta_{\text{ATS}} = \Omega_0$ [30, 31, 37], this places a constraint on the control field strength: the control field should be as weak as possible, in order to maximize absorption of $A(z, \tau)$ and population of $P(z, \tau)$, while still effecting the storage operation. The numerically optimized pulse areas as a function of τ_{FWHM} are shown in Fig. 2(b). In the non-adiabatic ($d\tau_{\text{FWHM}}\gamma \rightarrow 0$) and infinitely broadband ($\tau_{\text{FWHM}} \rightarrow 0$) limit, we determine through analytical approximations of Eqs. (1)-(3) that the optimal pulse area approaches $\theta = 4$, which is equivalent to the Autler-Townes splitting approximately matching the spectral bandwidth of

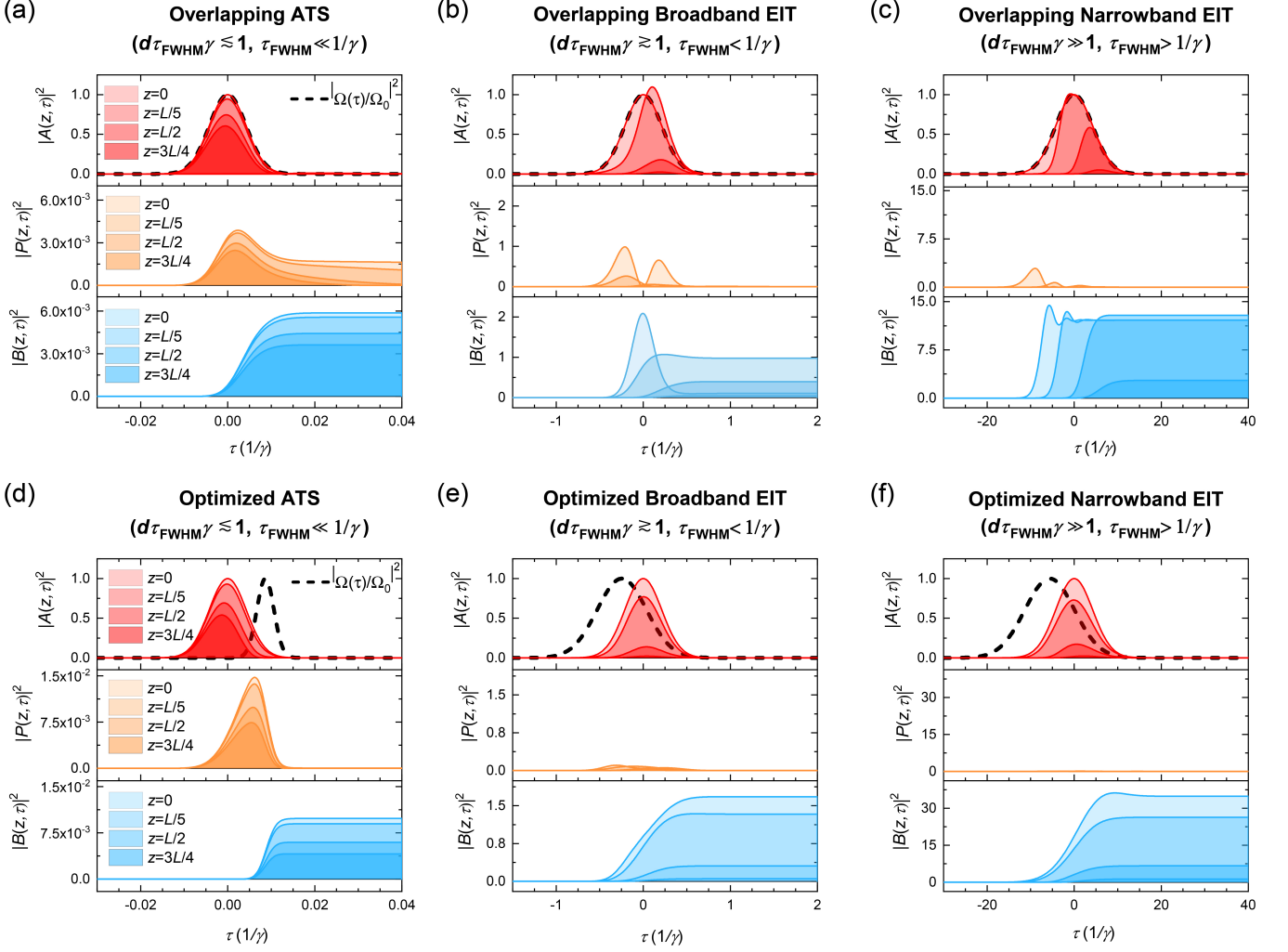


FIG. 3. Cross sections of normalized control field [$|\Omega(\tau)/\Omega_0|$, dashed black line], photonic signal [$A(z, \tau)$, shaded red], atomic polarization [$P(z, \tau)$, shaded orange], and spin wave [$B(z, \tau)$, shaded blue] intensities along the length of the medium at positions $z = 0, L/5, L/2, 3L/4$ along the atomic medium, for $d = 50$. The lightest shading corresponds to each field at the entrance of the medium ($z = 0$); shading gets progressively darker as z increases. In (a)-(c) we consider the pulse-area optimized overlapping signal and control fields of the same bandwidth and in (d)-(f) we consider Gaussian control fields optimized over pulse area, pulse duration and delay. The bandwidths considered correspond to (a,d) $\tau_{\text{FWHM}} = 0.01/\gamma$ (b,e) $\tau_{\text{FWHM}} = 0.5/\gamma$, and (c,f) $\tau_{\text{FWHM}} = 10/\gamma$.

the signal field: $\delta_{\text{ATS}} \approx \delta$. Physically, we provide the intuition that this value of the control field pulse area maximizes absorption of the signal field while still affecting significant—but not unit efficiency—transfer of population from $P(z, \tau)$ to $B(z, \tau)$. As shown in Fig. 3(a), the optimized control field strength leaves some population in $P(z, \tau)$ at the end of the storage operation, but nevertheless optimizes the storage efficiency.

As the signal field pulse duration increases in this restricted optimization scheme, the optimized storage efficiency exhibits a cusp while the control field pulse area exhibits a discontinuity [Fig. 2(b)]. This corresponds to an abrupt change in the optimal storage protocol from ATS using a $\theta \approx 2\pi$ pulse to mixed ATS-EIT using a $\theta \approx 4\pi$ pulse. The character ratio

$$\mathcal{C} = \frac{1}{\tau_s} \frac{\int_{-\tau_s/2}^{\tau_s/2} d\tau \int_0^L dz |P(z, \tau)|^2}{\int_0^L dz |B(z, \infty)|^2} \quad (6)$$

defined in Ref. [31], gives the ratio of the transient population that enters $P(z, \tau)$ during the storage period $\tau_s = 2.25\tau_{\text{FWHM}}$ to the population that ends up in $B(z, \tau)$ after the storage operation is completed. The normalized character ratio $\tilde{\mathcal{C}} \equiv \mathcal{C}/\mathcal{C}_0$ is defined using \mathcal{C} evaluated at the point where the optimized pulse area reaches $\theta = 2\pi$, which we identify as \mathcal{C}_0 . Where the storage efficiency exhibits a cusp, we find this normalized character ratio decreases abruptly from $\tilde{\mathcal{C}} = 0.9$ to $\tilde{\mathcal{C}} = 0.6$, indicating the transition from ATS stor-

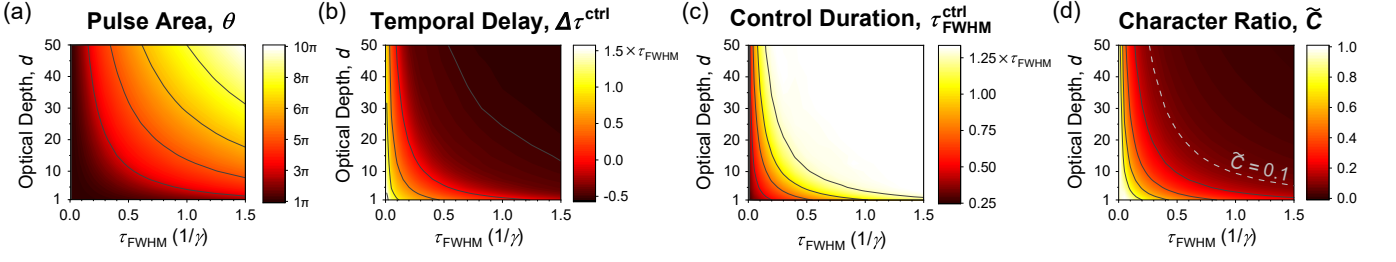


FIG. 4. (a)-(c) Optimized control field parameters obtained through the full Gaussian optimization scheme as a function of optical depth, d , and signal field duration, τ_{FWHM} . Positive (negative) delay, $\Delta\tau^{\text{ctrl}} > 0$ ($\Delta\tau^{\text{ctrl}} < 0$), refers to control fields that arrive after (before) the signal field. (d) Normalized character value calculated after optimization ($\tilde{C} \leq 0.1$ indicates EIT character).

age to mixed ATS-EIT storage. As the signal field pulse duration increases further, into the intermediate regime between broadband and narrowband memory operation ($\tau_{\text{FWHM}} \lesssim 1/\gamma$), the character ratio \tilde{C} decreases further toward the EIT regime ($\tilde{C} \leq 0.1$). In this region the storage efficiency and optimized pulse area exhibit a smooth fluctuation, which we identify as a transition in optimal storage protocol from “broadband EIT” [31] to conventional narrowband EIT. In broadband EIT, population is primarily transferred from $A(z, \tau)$ to $B(z, \tau)$ directly by adiabatic following of the dark instantaneous eigenstate, and the splitting of the excited state absorption feature exceeds the signal bandwidth ($\delta_{\text{ATS}} > \delta$). Contrary to the case in narrowband EIT [27], in broadband EIT the population that enters the $P(z, \tau)$ field through imperfect adiabatic elimination can actually *enhance* quantum storage through coherent population transfer [31]. This is evident in Fig. 3(b) as a significant population in $P(z, \tau)$ is transferred coherently to $B(z, \tau)$, and in Fig. 2(b) as the optimized control field area tends toward $\theta = 4\pi$, indicative of coherent population transfer.

Figure 3(c) shows atomic dynamics for the restricted optimization scheme in the adiabatic ($d\tau_{\text{FWHM}}\gamma \gg 1$) and narrowband ($\tau_{\text{FWHM}} > 1/\gamma$) regime, which are typical of the narrowband EIT protocol [27, 37]. In this case the population in $P(z, \tau)$ is reduced significantly, and the protocol does not benefit from control fields satisfying $\theta = n\pi$, where $n = 2, 4, 6, \dots$. Accordingly there are no oscillations in the storage efficiency shown in Fig. 2(a) and (b) beyond $\tau_{\text{FWHM}} = 1/\gamma$, and the optimized control field pulse area shown in Fig. 2(b) increases smoothly.

While the case of optimizing overlapping signal and control fields considered above has shown near-optimal storage efficiency to be possible using only Gaussian pulses, the region of near-optimality consists of a relatively small range of pulse bandwidths. We next consider a significantly improved scheme, wherein the Gaussian control field is optimized over pulse area, temporal delay relative to the signal field, and spectral bandwidth. In Fig. 2(a) and (b) we show the range of bandwidths that exhibit near-optimal storage efficiency can be increased

dramatically in the full optimization scheme (thick lines), even into the broadband regime. In particular, Fig. 2(a) shows storage efficiencies achieved with our full optimization scheme that saturate the optimal bound over the entire adiabatic region we investigate, representing enhancements as large as 15% (taken at $\tau_{\text{FWHM}} = 10/\gamma$ and $d = 1$; in general this enhancement increases with increasing τ_{FWHM}). In the non-adiabatic and broadband regimes we again observe significant enhancement, exceeding 30% for $d = 50$. In all cases, the amount of enhancement depends heavily on optical depth and the ratio of the signal field bandwidth and the excited state linewidth.

Figure 3(d)-(f) shows examples of the optimized atomic dynamics and Gaussian control fields we find through our full Gaussian optimization approach. In the ATS regime [Fig. 3(d)] we find the optimization continues to follow the intuition for the ATS protocol described above, where the optimized control field effects an ‘absorb-then-transfer’ process. In this regime, we find optimized control fields that arrive significantly delayed after the signal field, which allows for maximal linear absorption of $A(z, \tau)$ to $P(z, \tau)$ before the control field imparts a π -pulse to transfer population from $P(z, \tau)$ to $B(z, \tau)$. The optimized control fields arrive at the approximate time when the electric field of the signal changes sign, in agreement with the analysis of Refs. [35, 38, 39]. Importantly, the optimized control field is also significantly narrower in duration than the signal field, which again maximizes the duration of the absorption process before transfer. Optimized control fields of this form are in stark contrast to those found in the intermediate ($d\tau_{\text{FWHM}}\gamma \gtrsim 1$) and adiabatic regimes, shown in Fig. 3(e) and (f), respectively. In these regimes, the optimized control fields instead arrive before the signal field and are broader in duration. The physics of the optimized quantum memory interaction in these regions follows the EIT protocol: In both broadband and narrowband EIT, the optimized control field arrives before the signal field in order to open a transparency window at the signal frequency, and as the signal field propagates through the medium the transparency window is slowly closed (as the control field Rabi frequency decreases),

eventually stopping the signal field by the slow-light effect [27]. As shown in Fig. 3(e) and (f), control fields of this type reduce the population in $P(z, \tau)$ relative to the overlapping case [Fig. 3(b) and (c)], and maximize the population that arrives in $B(z, \tau)$ by adiabatic following.

Figure 4(a)-(c) provides the optimized parameters derived through our full Gaussian optimization approach, and Fig. 4(d) shows the crossover between ATS and EIT regimes, quantified by the character ratio \tilde{C} . In Fig. 4(a) we find optimized pulse areas that asymptote to $\theta = \pi$ in the non-adiabatic ($d\tau_{\text{FWHM}}\gamma \lesssim 1$) regime, where, in conjunction with the results of Fig. 4(b)-(c), we deduce that optimal storage is given by the ‘absorb-then-transfer’ optimized ATS protocol. As the storage operation becomes more adiabatic ($d\tau_{\text{FWHM}}\gamma$ increases), the control field pulse area increases. Figure 4(b) shows the optimized control field delays we calculate, where in the non-adiabatic, optimized-ATS regime we find positive temporal delay ($\Delta\tau^{\text{ctrl}} > 0$) corresponding physically to control fields that arrive *after* the signal pulse. In the adiabatic regime ($d\tau_{\text{FWHM}}\gamma \gg 1$), we find negative temporal delays that asymptote to around $-0.55\tau_{\text{FWHM}}$. A similar distinction between non-adiabatic and adiabatic regimes is observed in the optimized values of the control duration, Fig. 4(c), where in the non-adiabatic regime we observe control fields shorter than the corresponding signal field ($\tau_{\text{FWHM}}^{\text{ctrl}} < \tau_{\text{FWHM}}$), and in the adiabatic regime we observe longer control fields ($\tau_{\text{FWHM}}^{\text{ctrl}} > \tau_{\text{FWHM}}$) that asymptote to $\sim 1.33\tau_{\text{FWHM}}$ in duration. In Fig. 4(d), we calculate the normalized character ratio \tilde{C} for each set of optimized parameters, where we normalize by the largest value of C in the region we simulate. $\tilde{C} \leq 0.1$ marks the boundary between EIT behavior and mixed EIT-ATS behavior, and $\tilde{C} = 1$ represents pure ATS storage.

IV. CONCLUSION AND FUTURE WORK

In this work we have presented a quantitative and qualitative exploration of Λ -type quantum memory with Gaussian optical fields. We consider the naïve scheme of overlapping signal and control fields as well as a scheme that employs fully optimized Gaussian control fields,

where optimization occurs over control field pulse area, temporal delay relative to the signal field, and bandwidth. In the adiabatic and narrowband regime, we recover the physical intuition present in the EIT-based quantum memory protocol, and in the non-adiabatic, broadband regime we derive novel physical intuition for ATS-based quantum memory. Through this simple optimization, we have shown that under certain conditions control fields with Gaussian temporal envelope are sufficient for optimal quantum memory operation.

In considering both adiabatic and non-adiabatic timescales, we derive the result that for a given quantum memory described by excited state linewidth $\Gamma = 2\gamma$ and optical depth d , there exists either a single Gaussian bandwidth (without full optimization) or a finite range of bandwidths (with full optimization) where the memory efficiency is maximized. The converse of this statement is also true, which we anticipate will inform emerging quantum memory research with Gaussian pulses: the use of a given quantum memory with Gaussian signal and control fields with a signal photon bandwidth outside of the optimized range calculated through our analysis necessarily implies sub-optimal memory performance.

In this work we restrict ourselves to the widely available resource of Fourier-transform limited pulses, where pulse duration and bandwidth are Fourier-transform pairs and accordingly only describe one degree of freedom subject to optimization. Future work may consider non-adiabatic shape-based optimization [40] informed by these results, as well as optimization via chirped optical fields, which expands the toolbox for optimization of Gaussian quantum memory and has been explored in other memory protocols [41–43]. In addition, in Ref. [34] we consider more completely the present case, where optimization over all combinations of pulse area, delay, and duration are explored in more detail.

V. ACKNOWLEDGEMENTS

We gratefully acknowledge helpful discussion provided by Yujie Zhang, Xinan Chen, Sehyun Park, and Elizabeth Goldschmidt, as well as support from NSF Grant Nos. 1640968, 1806572, 1839177, and 1936321 and NSF Award DMR-1747426.

-
- [1] J. Nunn, N. K. Langford, W. S. Kolthammer, T. F. M. Champion, M. R. Sprague, P. S. Michelberger, X.-M. Jin, D. G. England, and I. A. Walmsley, *Phys. Rev. Lett.* **110**, 133601 (2013).
 - [2] F. Kaneda and P. G. Kwiat, *Science Advances* **5**, eaaw8586 (2019).
 - [3] N. Sangouard, C. Simon, H. de Riedmatten, and N. Gisin, *Rev. Mod. Phys.* **83**, 33 (2011).
 - [4] L.-M. Duan, M. Lukin, J. Cirac, and P. Zoller, *Nature* **414**, 413 (2001).
 - [5] E. Knill, R. Laflamme, and M. G., *Nature* **409**, 46 (2001).
 - [6] K. F. Reim, J. Nunn, V. O. Lorenz, B. J. Sussman, K. C. Lee, N. K. Langford, D. Jaksch, and I. A. Walmsley, *Nat. Photonics* **4**, 218 (2010).
 - [7] C. Simon, *et al.*, *Eur. Phys. J. D* **58**, 1 (2010).
 - [8] I. Novikova, A. V. Gorshkov, D. F. Phillips, A. S. Sørensen, M. D. Lukin, and R. L. Walsworth, *Phys. Rev. Lett.* **98**, 243602 (2007).
 - [9] A. V. Gorshkov, A. André, M. Fleischhauer, A. S. Sørensen, and M. D. Lukin, *Phys. Rev. Lett.* **98**, 123601 (2007).

- (2007).
- [10] A. V. Gorshkov, T. Calarco, M. D. Lukin, and A. S. Sørensen, *Phys. Rev. A* **77**, 043806 (2008).
 - [11] H. Nakao and N. Yamamoto, *J. Phys. B* **50**, 065501 (2017).
 - [12] I. Novikova, N. B. Phillips, and A. V. Gorshkov, *Phys. Rev. A* **78**, 021802 (2008).
 - [13] N. B. Phillips, A. V. Gorshkov, and I. Novikova, *Phys. Rev. A* **78**, 023801 (2008).
 - [14] J. Guo, X. Feng, P. Yang, Z. Yu, L. Q. Chen, C.-H. Yuan, and W. Zhang, *Nat. Commun.* **10**, 148 (2019).
 - [15] M. Hosseini, B. Sparkes, G. Campbell, P. Lam, and B. Buchler, *Nat. Commun.* **2**, 174 (2011).
 - [16] Y.-H. Chen, M.-J. Lee, I.-C. Wang, S. Du, Y.-F. Chen, Y.-C. Chen, and I. A. Yu, *Phys. Rev. Lett.* **110**, 083601 (2013).
 - [17] Y.-W. Cho, G. T. Campbell, J. L. Everett, J. Bernu, D. B. Higinbottom, M. T. Cao, J. Geng, N. P. Robins, P. K. Lam, and B. C. Buchler, *Optica* **3**, 100 (2016).
 - [18] Y.-F. Hsiao, P.-J. Tsai, H.-S. Chen, S.-X. Lin, C.-C. Hung, C.-H. Lee, Y.-H. Chen, Y.-F. Chen, I. A. Yu, and Y.-C. Chen, *Phys. Rev. Lett.* **120**, 183602 (2018).
 - [19] Y. Wang, J. Li, S. Zhang, K. Su, Y. Zhou, K. Liao, S. Du, H. Yan, and S.-L. Zhu, *Nat. Phys.* **13**, 346 (2019).
 - [20] D. G. England, P. J. Bustard, J. Nunn, R. Lausten, and B. J. Sussman, *Phys. Rev. Lett.* **111**, 243601 (2013).
 - [21] P. J. Bustard, R. Lausten, D. G. England, and B. J. Sussman, *Phys. Rev. Lett.* **111**, 083901 (2013).
 - [22] D. G. England, K. A. G. Fisher, J.-P. W. MacLean, P. J. Bustard, R. Lausten, K. J. Resch, and B. J. Sussman, *Phys. Rev. Lett.* **114**, 053602 (2015).
 - [23] P. S. Michelberger, T. F. M. Champion, M. R. Sprague, K. T. Kaczmarek, M. Barbieri, X. M. Jin, D. G. England, W. S. Kolthammer, D. J. Saunders, J. Nunn, and I. A. Walmsley, *New J. Phys.* **17**, 043006 (2015).
 - [24] S. E. Thomas, J. H. D. Munns, K. T. Kaczmarek, C. Qiu, B. Brecht, A. Feizpour, P. M. Ledingham, I. A. Walmsley, J. Nunn, and D. J. Saunders, *New J. Phys.* **19**, 0063034 (2017).
 - [25] E. Saglamyurek, N. Sinclair, J. Jin, J. A. Slater, D. Oblak, F. Bussières, M. George, R. Ricken, W. Sohler, and W. Tittel, *Nature* **469**, 512 (2011).
 - [26] K. A. G. Fisher, D. G. England, J.-P. W. MacLean, P. J. Bustard, K. Heshami, K. J. Resch, and B. J. Sussman, *Phys. Rev. A* **96**, 012324 (2017).
 - [27] M. Fleischhauer and M. D. Lukin, *Phys. Rev. A* **65**, 022314 (2002).
 - [28] A. I. Lvovsky, B. C. Sanders, and W. Tittel, *Nat. Photonics* **3**, 706714 (2009).
 - [29] A. V. Gorshkov, A. André, M. D. Lukin, and A. S. Sørensen, *Phys. Rev. A* **76**, 033805 (2007).
 - [30] A. R. K. H. . L. J. L. Erhan Saglamyurek, Taras Hrushevskiy, *Nat. Photonics* **12**, 774 (2018).
 - [31] A. Rastogi, E. Saglamyurek, T. Hrushevskiy, S. Hubele, and L. J. LeBlanc, *Phys. Rev. A* **100**, 012314 (2019).
 - [32] E. Saglamyurek, T. Hrushevskiy, L. Cooke, A. Rastogi, and L. J. LeBlanc, *Phys. Rev. Research* **1**, 022004 (2019).
 - [33] M. O. Scully and M. S. Zubairy, *Quantum Optics* (Cambridge University Press, 1997).
 - [34] K. Shinbrough, B. D. Hunt, and V. O. Lorenz (2020), *Manuscript in preparation*.
 - [35] A. J. A. Carvalho, R. S. N. Moreira, J. Ferraz, S. S. Vianna, L. H. Acioli, and D. Felinto, *Phys. Rev. A* **101**, 053426 (2020).
 - [36] J. Nunn, I. A. Walmsley, M. G. Raymer, K. Surmacz, F. C. Waldermann, Z. Wang, and D. Jaksch, *Phys. Rev. A* **75**, 011401 (2007).
 - [37] L. Giner, L. Veissier, B. Sparkes, A. S. Sheremet, A. Nicolas, O. S. Mishina, M. Scherman, S. Burks, I. Shomroni, D. V. Kupriyanov, P. K. Lam, E. Giacobino, and J. Laurat, *Phys. Rev. A* **87**, 013823 (2013).
 - [38] L. S. Costanzo, A. S. Coelho, D. Pellegrino, M. S. Mendes, L. Acioli, K. N. Cassemiro, D. Felinto, A. Zavatta, and M. Bellini, *Phys. Rev. Lett.* **116**, 023602 (2016).
 - [39] J. E. Rothenberg, D. Grischkowsky, and A. C. Balant, *Phys. Rev. Lett.* **53**, 552 (1984).
 - [40] J. Nunn, *Quantum Memory in Atomic Ensembles*, Ph.D. thesis, University of Oxford (2008).
 - [41] J. Minář, N. Sangouard, M. Afzelius, H. de Riedmatten, and N. Gisin, *Phys. Rev. A* **82**, 042309 (2010).
 - [42] G. Demeter, *Phys. Rev. A* **89**, 063806 (2014).
 - [43] X. Zhang, A. Kalachev, and O. Kocharovskaya, *Phys. Rev. A* **90**, 052322 (2014).